Check for updates

BIOLOGICAL RESPONSE OF BIPHASIC HYDROXYAPATITE/TRICALCIUM PHOSPHATE SCAFFOLDS INTENDED FOR LOW LOAD-BEARING ORTHOPAEDIC APPLICATIONS

F. Baghbani [1], F. Moztarzadeh [1,*], A. Gafari Nazari [2], A.H. Razavi Kamran [1], F. Tondnevis [1], N. Nezafati [1], M. Gholipourmalekabadi [3], M. Mozafari [1]

[1] Biomaterials Group, Faculty of Biomedical Engineering (Centre of Excellence), Amirkabir University of Technology, P. O. Box: 15875-4413, Tehran, Iran
[1] Department of Mechanical and Industrial Engineering, University of Brescia, Via Branze 38, 25123 Brescia, Italy
[3] Department of Biotechnology, Shahid Beheshti University of Medical Sciences. tehran, Iran

* Author to whom correspondence should be addressed:
E-mail: moztarzadeh@aut.ac.ir, Fax: (+98-21) 64542370

ABSTRACT

In this study, a calcium phosphate scaffold of hydroxyapatite (HAp) and dicalcium phosphate dihydrate (DCPD) for application in osteoconductive and osteoinductive scaffolds was synthesized and characterized. The important note is that the prepared composites converted to HAp/tricalcium phosphate (TCP) after heat-treatment. This class of composites is interesting because porous HAp/TCP generally degrade more rapid than HAp due to the increased resorption rate of TCP. According to the obtained results, the values of elastic modulus, compressive strength and density of the samples reduced with increasing the percentage of the DCPD phase. It is worth mentioning that the mechanical properties of the prepared samples were near the natural compact bone. The samples were examined in vitro to confirm the apatite forming ability of the composites. Also, in vivo examination in a rabbit model was employed. After fully observation it was concluded that new bone formed on the pore walls, as osteoids and osteoclasts were evident two months postoperatively. Based on the obtained results, the prepared scaffolds seem to be a promising biomaterial for low weight bearing orthopaedic applications.

Keywords: Biphasic composites; Hydroxyapatite; Tricalcium phosphate; In vitro; In vivo

1. INTRODUCTION

Bone tissue engineering and regenerative medicine is a new research area with clinical applications in bone replacement on orthopedic defects, bone neoplasia and tumors, pseudoarthrosis treatment, stabilization of spinal segments, as well as in maxillofacial, craniofacial, orthopedic, reconstructive, trauma and neck and head surgery [1-6]. It may provide solutions for generating a new bone tissue with good functional and mechanical qualities, reducing the risks and expenses of using autografts, allografts and metals [7-10].

During the last decades, different biomaterials of biological or synthetic origin have been designed with aim of acting as extracelular matrix composite scaffolds for new bone formation. Meanwhile, clinical uses require a series of biomaterial properties such as bioactivity, osteoconduction, osteoinduction, biocompatibility and biodegradation [11–14]. Biomaterials play a key role in several biomedical applications, and it is imperative that both the materials and biological aspects are clearly understood for attaining successful biological outcome. Among biomaterials, calcium phosphates (CaP) are the most ubiquitous family of bioceramics well known for their use in biological applications [15].

The chemical composition of calcium phosphate bioceramics is roughly equivalent to that of the inorganic matrix of human bone and is found to be the most suitable as implant materials. Major phase found in bone is hydroxyapatite (HAp, $Ca_{10}(PO_4)_6(OH)_2$) and the other commonly known phases are octacalcium phosphate (OCP), tricalcium phosphate (TCP), dicalcium phosphate dihydrate (DCPD, $CaHPO_4{\bullet}2H_2O$) and dicalcium phosphate DCP bioceramics. Hydroxyapatite (HAp) is one of the frequently used bioceramics for bone and dental tissues reconstitution, which has excellent biocompatibility with hard tissues [16,17], and high osteoconductivity and bioactivity despite its low degradation rate [18], mechanical strength and osteoinductive potential [19,20]. It has also neither antigenicity nor cytotoxicity [21,22]. In addition, it seems that using DCPD in bone tissue engineering is interesting, and a large number of studies have reported the advantages of using DCPD bioceramic

in bone tissue engineering applications [23]. For instance, a report indicated that the mechanisms of DCPD growth and dissolution were of interest because of the importance of this calcium phosphate in dental and bone regeneration applications [24]. The properties of the anhydrous and hydrated salts dicalcium phosphate, $CaHPO_4$ and $CaHPO_4 \bullet 2H_2O$, have been studied for many years as their mineral forms, monetite and brushite. As members of the series of calcium phosphates, they have considerable biological importance with respect to the biomineralization processes in bones and teeth, and find practical uses in dental cements and restorative materials. It is also important to point out that the degradability of different calcium phosphates varies with the ratio of Ca/P, with the highest being that of DCPD, which usually results in the most extensive bone remodeling around the scaffold [25-29].

Previous studies have used different forms of HAp but concerns have been raised regarding the limited degradation properties of this material [30,31]. Therefore, biphasic composites of HAp and biodegradable material, like HAp/TCP have been studied as an alternative to HAp ceramics. Porous biphasic calcium phosphate composite bioceramics are expected to accommodate bone grow and this characteristic provides osteoconductive properties.

Porous bioceramics of HAp/TCP and HAp/DCPD generally biodegrade faster than bioceramics made of HAp due to the increased resorption rates relative to HAp implants of similar structures [32]. The bioresorbability of calcium phosphate ceramics appears to be dependent on their chemical/crystal composition, and on the environment of the implantation site [33]. Jarcho [34] has proposed the existence of two different biologic resorption pathways: one involving solution-mediated processes and the second involving cell-mediated processes. Contrary to expectations, the material more closely resembling the body's own hard tissue component (HAp) was found to dissolve much more slowly than many calcium phosphates not naturally occurring in bone, when similar ceramic structures and degrees of purity were used [35]. It can be stated that implants of crystalline HAp have lower tendency to bioresorb because of their chemistry and their small surface area.

Many methods to prepare porous three-dimensional scaffolds have been developed in tissue engineering including gas forming, three-dimensional printing, phase separation, emulsion freeze-drying, porogen-leaching etc. In this study, porous composite structures of HAp/DCPD bioceramics containing different percentages of each component were designed using polyurethane foam template to evaluate the effect of DCPD addition on the chemical and mechanical properties of the final composites. However, after heat-treatment DCPD converted to TCP phase. Finally, *in vitro* and *in vivo* examinations were performed to evaluate the biological responses of the prepared samples.

2. MATERIALS AND METHODS

2.1. Preparation of composites

For the synthesis of composite samples, commercially purified HAp and DCPD powders (Merck, Germany) were used. Powders of HAp/DCPD, with different weight ratios, were prepared in a planetary ball mil (Retch PMA, Brinkman, USA) (zirconium balls with the average size of 15 mm) for 30 min to ensure homogeneity. The specific surface area was determined by 15-point BET measurement (Micromeritics Gemini 2360). Then, the powders (P) were suspended in distilled water (W) at ratio of P/W = 55% w/v, and different additives such as (colloidal silica, three poly phosphate and carboxy methyl cellulose) were mixed to the HAp/DCPD solution for 24 h to obtain a suitable bioceramic slurry. The porous scaffolds with different amount of HAp and DCPD (see Table 1) were fabricated by polyurethane foam reticulate method. Polyurethane foam templates were purchased from Safoam (80 ppi, Iran). Typically, the polyurethane foam templates were replicated using the slurry by a repeated dipping-and-drying process. The samples were then air-dried, and after drying, the samples were heated to 1,050 ºC on a strict schedule, which minimized disruption during pyrolysis and allowed the bioceramic to achieve a high density. This heating schedule consisted of a heating rate of 0.5 ºC/min up to 800 ºC, held at this temperature for 1 h, then rapid heating of 5 ºC/min from 800 to 1,050 ºC, held at 1,050 ºC for 3 h, and then cooled in the furnace. Fig. 1 shows the prepared composite samples using polyurethane foam template.

2.2. Preparation of SBF

Reagent-grade chemicals NaCl, $NaHCO_3$, KCl, $K_2HPO_4.3H_2O$, $MgC_{l2}.6H_2O$, CaC_{l2}, trishydroxymethylaminomethane [Tris-buffer, $(CH_2OH)_3CNH_2$], and 1 N HCl as required materials for preparation of SBF, were purchased from Merck Inc. The SBF solution was prepared by dissolving reagent-grade NaCl, KCl, NaHCO3, $MgCl_2.6H_2O$, $CaCl_2$ and KH_2PO_4 into distilled water and buffered at pH=7.25

Table 1: Prepared HAp/DCPD composite samples

Composite sample	HAp wt%	DCPD wt%
C1	100	0
C2	90	10
C3	80	20
C4	70	30
C5	60	40

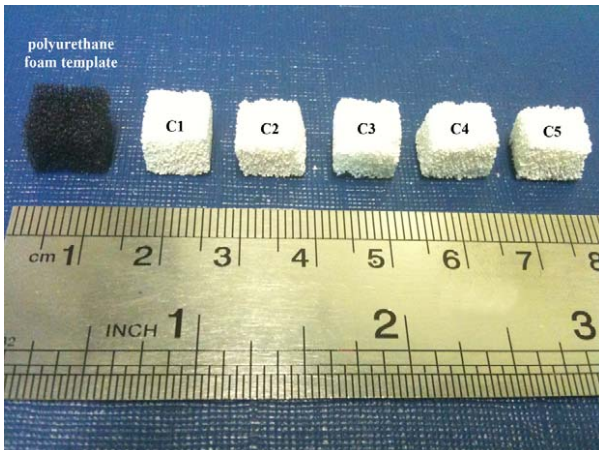

Fig. 1: Prepared composite samples using polyurethane foam template.

with Tris-buffer and HCl 1N at 37 °C [26].

2.3. Sample characterization

2.3.1. XRD analysis

The samples surfaces were analyzed by XRD with Siemens-Brucker D5000 diffractometer. This instrument works with voltage and current settings of 40 kV and 40 mA respectively and uses Cu-Kα radiation (1.540600 Å). For qualitative analysis, XRD diagrams were recorded in the interval 10°≤2θ≤50°at scan speed of 2°/min.

2.3.2. FTIR analysis

The samples were examined by FTIR with Bomem MB 100 spectrometer. For IR analysis, 1 mg of the scraped samples were carefully mixed with 300 mg of KBr (infrared grade) and palletized under vacuum. Then the pellets were analyzed in the range of 400-4000 cm-1 with 4 cm-1 resolution averaging 120 scans.

2.3.3. SEM analysis

The morphology and microstructure of the synthesized samples were evaluated using SEM. The samples were coated with a thin layer of Gold (Au) by sputtering (EMITECH K450X, England) and then the morphology of them were observed on a scanning electron microscope (SEM-Philips XL30) that operated at the acceleration voltage of 15 kV.

2.4. Density, porosity and pore size measurement

For density and porosity measurements, the sintered specimens were initially subjected to ultra-sonic washing in distilled water for a few minutes. After drying the samples in a stagnant air oven at 90 °C, their dry weights were recorded. The porous specimens were then boiled in distilled water for about 3 h, and allowed to cool in water for 24 h. Wet weight in air and wet weight suspended in water were determined using an analytical balance (Precisa, 300S, Switzerland). Bulk density, apparent porosity, and volume fraction of porosity were calculated in our samples using the below formula (1), (2) and (3):

$$\text{Bulk density} = D/(W - S) \quad (1)$$

$$\text{Apparent porosity} = (W - D)/(W - S) \quad (2)$$

$$\text{Volume fraction of porosity} = 1 - (\text{bulk density}/\text{theoretical density}) \quad (3)$$

where W is the wet weight, D is the dry weight, and S is the wet weight suspended in water. In addition, the average pore size was calculated from micrographs taken using SEM.

2.5. Mechanical behaviour

For analyzing the mechanical behaviour of the composite samples, they were supplied in the form of cylinders with a mean diameter of 3.4 ± 0.5 mm, which were filled down to a length of 6.3 ± 0.7 mm. All mechanical testing was performed using a Zwick/Roell 2005 with a crosshead speed of 0.01 mm/s. The compressive strength and modulus of elasticity were determined from mechanical test recordings. The modulus of elasticity was determined from the slope of the linear portion of the stress-strain curve.

2.6. Biological evaluation

2.6.1. In vitro study in SBF

We performed in vitro studies by immersion of the samples in SBF at a concentration of 1 mg sample per milliliter of the fluid at 37 °C for different time periods. All the reacted solutions were saved for ICP-AES (Varian Co., USA) analysis of Ca to measure ionic concentration in the SBF solutions. In addition, pH of the SBF solutions were measured by a calibrated pH meter every step and using a Corning pH meter 320.

2.6.2. In vivo implantation procedure, histological testing

For in vivo implantation, all specimens were sup-

plied in the form of cylinders with a mean diameter of 3.4 ± 0.5 mm, which were filled down to a length of 6.3 ± 0.7 mm. Specimens were sterilized with ethylene oxide gas before implantation. Then, the specimens were inserted into defects made using a saline-cooled, diamond-tipped 3.5 mm trephine in the medial femoral condyle of rabbits (mature male New Zealand rabbits weighting about 3.5 kg). The rabbits were sacrificed for the assessment of the biomechanical properties of the implanted specimens and the observation of bone ingrowth by light microscopy. For histological examination, samples were decalcified in 10% formalin solution and sectioned into pieces 5~6 mm thick, then stained with hematoxylin-eosin and masons trichrome stain. The sections were examined with a light microscope. The amount of fibrous tissue, new bone formation, and the presence of remodeling were qualitatively assessed. The presence of new lamellar bone and osteoclasts along the trabeculae of the newly formed woven bone were considered signs of remodeling.

2.7. Statistical analysis

All experiments were performed in fifth replicate. Tukey's HSD multiple comparison testing was used to determine the significance of the deviations in the strength and modulus of each sample. For all statistical tests, a p value of less than 0.05 was considered to be significant. All statistical analyses were performed with the software program SPSS for Windows, version 9 (SPSS Inc., Chicago, IL, USA).

3. RESULTS AND DISCUSSION

3.1. XRD analysis

Fig. 2 shows the XRD patterns of the prepared composite samples. As it can be seen in this figure, the first sample (C1) shows the main characteristic peaks of HAp (Ca10(PO4)6(OH)2, JCPDS No. 09-0432) as the major phase, with a minor phase of β-tricalcium phosphate (Ca3(PO4)2, β-TCP, JCPDS No. 09-0169). It is also obvious that by further addition of the brushite phase to the composite samples the main characteristic peaks of β-TCP became more appear and finally for the C5 sample, β-TCP was the major phase. As the main product of pyrolysis of brushite at higher than 600 ºC is calcium pyrophosphate, and calcium pyrophosphate at higher than 1000 ºC react with HAp to form β-TCP, as shown in the following reactions (4) and (5):

$$2HPO_4^{-2} \rightarrow P_2O_7^{-4} + H2O \quad (4)$$

$$P_2O_7^{-4} + OH- \rightarrow 2PO_4^{-3} + H^2O \quad (5)$$

According to Hench [36], at higher temperatures other phases such as β-TCP or $Ca_4P_2O_9$ (tetracalcium phosphate, C4P) are present. Also, it is worth mentioning that this unhydrated high-temperature calcium phosphate phases interact with water, or body fluids, at 37°C to form HAp. The HAp layers form on exposed surfaces of β-TCP by the following reaction (6):

$$4Ca_3(PO_4)_2+2H_2O \rightarrow Ca_{10}(PO_4)_6(OH)_2 +2Ca^{2+}+2HPO_4^{2-} \quad (6)$$

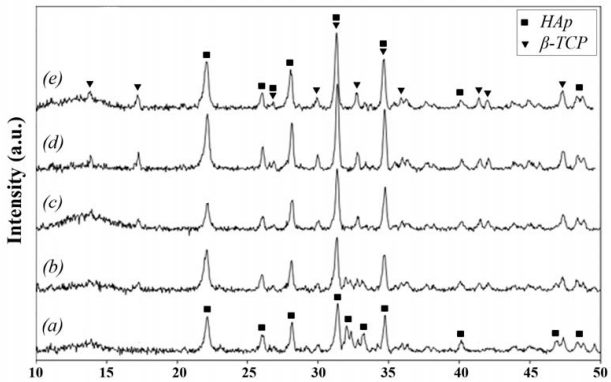

Fig. 2: XRD patterns of the composite samples (a) C1, (b) C2, (c) C3, (d) C4 and (e) C

3.2. FTIR analysis

Fig. 3 shows the FTIR spectra, in the 400–4000 cm^{-1} spectral range, of the prepared composite samples. The C1 sample exhibited five important infrared bands of HAp located at: 560, 605, 710, 1040, 1640 and 3479 cm^{-1}. The characteristic PO_4^{3-} and OH- absorption bands of HAp were observed in the as-dried sample along with the additional broad bands at 1640 cm^{-1} and 3479 cm^{-1} from the adsorbed H_2O. In addition, the band at 1040 cm^{-1} arises from υ_3 PO_4, the bonds at 560 and 605 cm^{-1} arise from υ_4 PO_4. The FTIR analysis showed all typical absorption characteristics of the HAp powder, and according to these explanations, it is obvious that the synthesized powder is certainly HAp. The weak absorption peak at 880 cm^{-1} was assigned to the P–O–H vibration in the HPO_4^{2-} group [37], which exists in non-stoichiometric HAp. It is worth mentioning that by further addition of brushite powder to the composite samples, the OH- absorption band disappeared and the spectrum obtained was characteristic of β-TCP. Also, the obtained results from the FT-IR spectrum of composite samples became similar to that of obtained results from XRD patterns [38].

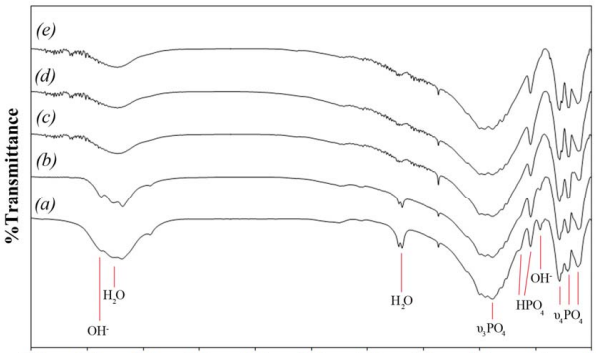

Fig. 3: FTIR patterns of the composite samples (a) C1, (b) C2, (c) C3, (d) C4 and (e) C5

3.3. SEM observations

In this study, SEM was used to observe the morphology of scaffolds microstructure. The low and high magnifications of SEM micrographs captured from the top view of composites which are shown in Fig. 4 (a) and (b). The observations indicate a network of interconnected pores. Also, the composites were porous with non-parallel aligned, and the pores were close to spherical shapes with the size ranged from 100 to 200 µm which can be desirable for bone cell growth [39].

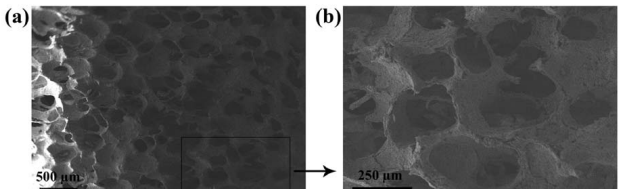

Fig. 4: SEM micrographs captured from the top view of composites (a) low and (b) high magnification

3.4. Mechanical properties

Generally, an ideal tissue engineering implant should be biocompatible and highly porous with adequate mechanical properties. For this purpose, the prepared nanocomposite samples were tested to determine the effects of using second phase on the mechanical properties of the samples. For natural spongy bone the elastic constant (E) is in the range of 20 to 500 MPa, compressive yield strength (σyeild) in the range of 4 to 12 MPa, and density (ρ) from 0.14 to 1.2 g/cm^3. Also, these mechanical indices are different for compact bone which the elastic constant (E) is in the range of 3× 10^3 to 30 × 10^3 MPa, compressive yield strength (σ_{yeild}) in the range of 130 to 180 MPa, and density (ρ) from 1.8 to 2 g/cm^3 [40,41]. In addition, Fig. 5 (a), (b) and (c) show the elastic constant (E), compressive yield strength (σ_{yeild}) and density (ρ) of the prepared samples, respectively. As it can be seen in this figure, the values of elastic modulus, compressive strength and density of the samples reduced with increasing the percentage of the second phase.

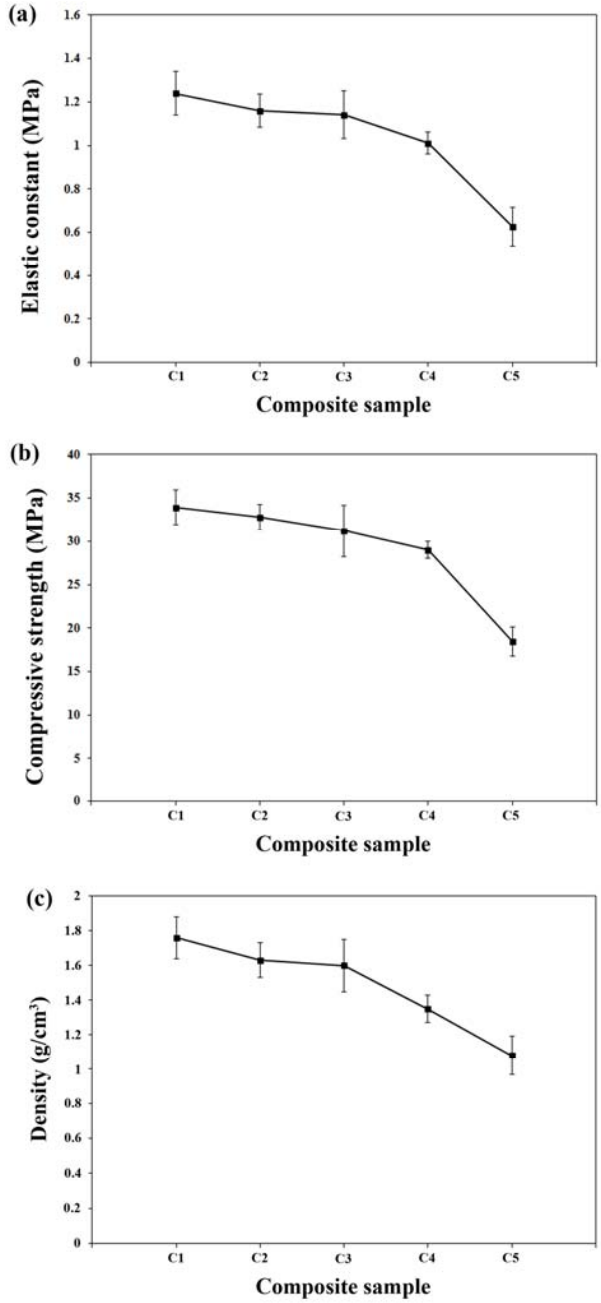

Fig. 5: Mechanical properties of the prepared samples (a) elastic constant, (b) compressive yield strength and (c) density

In addition, elastic modulus values varied from 0.6 to about 1.2 GPa, σ_{yeild} values varied from 15 to 35 MPa, and density values varied from 1 to 1.8 g/cm^3. Also, according to Fig. 6 which shows the percentage of porosity of the samples indicated that the porosity values increased by further addition of the second phase, and it is worth mentioning that these materials seems to be suitable for low load-bearing orthopaedic applications.

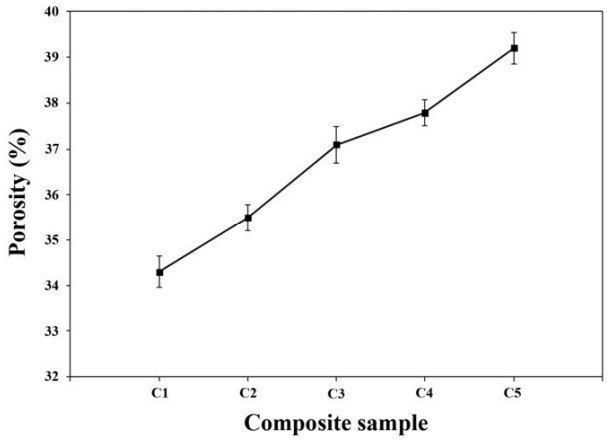

Fig. 6: Porosity percentages of different prepared composite samples

3.5. In vitro characterization

3.5.1. Changes in SBF composition

Fig. 7 shows the variations of Ca concentration in the SBF solution for various periods, measured by ICP-AES, versus immersion time. When the composites react with SBF, both chemical and structural changes occur as a function of time within their surfaces [34] and accumulation of dissolution products causes some changes in both chemical composition and pH of solution. As it can be seen in all the cases, Ca concentration in the solution increased continuously during the first days of immersion. In addition, pH variation with time increased from 7.4 to 8 during the 4 weeks of immersion and then pH increased slowly up to 8.3 until week 8. Bioactive scaffolds from calcium phosphate bioceramics elaborated under pressure and under temperature treatment of $Ca(NO_3)_2$, H_3PO_4, NH_4OH and H_2O [42]. As can be seen in the SEM micrographs (see Fig. 4), the structure of samples are clearly porous. We can also distinguish the microporosities (<10 µm) which permit diffusion of ions and fluids from macroporosities (100-600 µm) which permit cellular colonization. The bioactivity process of different bioactive materials was studied *in vitro* and *in vivo* [43]. Here, the bioactivity process occurs under an acidic attack with H^+ at the material surface. This leads the dissolution of calcium phosphate crystals and a high release of Ca^{2+}, PO_4^{3-} [44]. The concentration of Ca and P increase in the surrounding fluids and this supersaturation induces re-precipitation of apatite crystals [45]. These apatite crystals may also be incorporated by Ca^{2+}, Mg^{2+}, CO^{3-}, PO_4^{3-} or organic molecules present in the surrounding fluids [46]. This dissolution re-precipitation process leads to the formation of a carbonated apatite layer at the material surface and permits a chemical bond with newly formed bone. Solubility of calcium phosphate base bioactive materials vary with different factors: porosity, grain size, crystallinity, sintering temperature and so on [47,48]. For instance, an increase in the sintering temperature leads to an increase of the HAp crystal size and finally reduces its solubility. On the other hand, the solubility increases with the porosity and pores size.

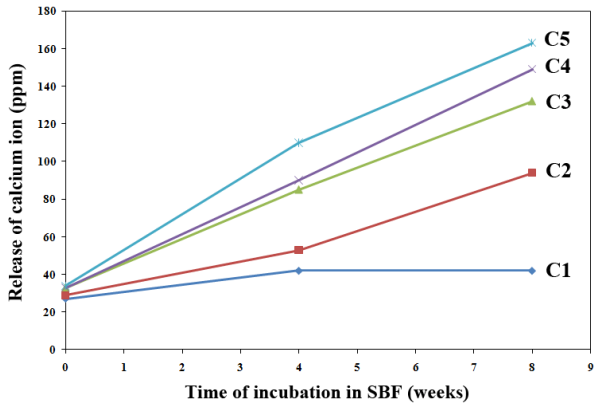

Fig. 7: Variations of Ca concentration for different samples in the SBF solution for various periods measured by ICP-AES

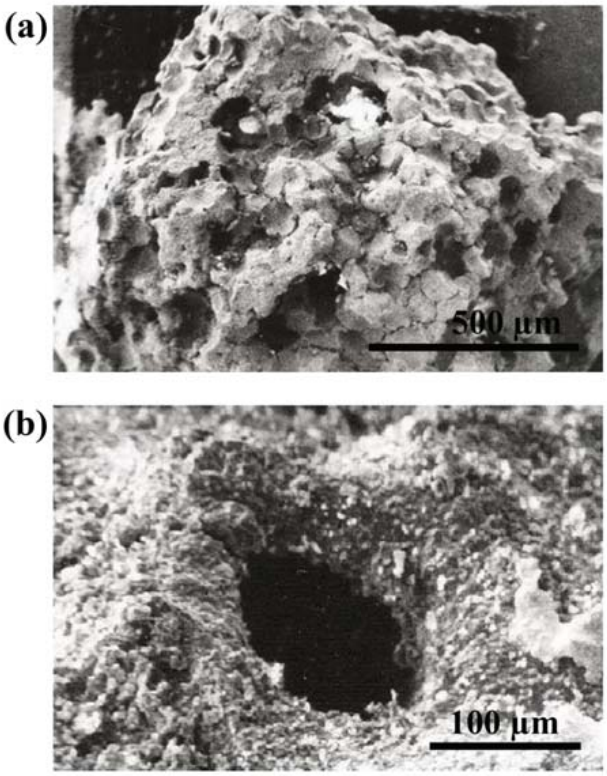

Fig. 8: SEM micrographs of the scaffolds after immersion in SBF (a) low and (b) high magnification

3.5.2. SEM observations after immersion in SBF solution

Herein, apatite was incorporated onto the surface of the scaffolds in situ via the SBF technique. Fig. 8 (a)

and (b) show the SEM micrographs of the scaffolds after immersion for 2 weeks. According to the observations, scattered and small particles were covered on the surface of the scaffold pore walls after immersion which is shown in Fig. 8 (a). Substantial amount of apatite microparticles formed on the surfaces of the pore walls throughout the scaffold. After that the whole inner pore wall surfaces of the scaffold were covered by a layer of apatite, and the underlying surfaces were not clearly observable. Also, it is predictable that a longer immersion time of the scaffolds led to more apatite formation.

3.6. In vivo evaluations

Apatite mineralization of bioactive materials is thought to be an important phenomenon in the chemical interactions between the implant materials and the bone tissue, which ultimately affects the *in vivo* osteogenesis of the bone grafting materials. Fig. 9 shows the optical micrograph of *in vivo* examination of sample C5 after two months. According to the obtained results, no inflammation, tissue necroses, or tissue rejection was observed after implantation. Generally, during the *in vivo* process at one-month post operation, fibrous connective tissue and blood vessels grow into the macropores, contributing to the early fixation of the specimens. However, there is no new bone formation in the macropores and few macrophages are detected on the macropore surfaces. Herein, new bone formation occurred on the surface and macropore walls of specimens, as osteoids and osteoclasts were evident at two months postoperatively. The fusion of the specimen and the host bone was realized through the bonding of new bone three months postoperatively. The new bone occupied most of the macropore spaces, and a new bone tissue layer developed on the inside surface of the specimen and replaced the previously mentioned connective tissue membrane two months postoperatively. In general, it is expected that in such implantation, osteoblasts develop one month postoperatively, bone marrow starts to develop in new bone tissues at two months postoperatively, and bone tissue tends to mature with the development of osteocytes and bone marrow greater than two months postoperatively. Dissolution properties of the biphasic HAp/TCP had important effects on bone formation at various implantation periods. The further degradation of the biphasic specimen provided rich Ca and P ions for new bone formation, and the thinner regions of the macropore walls disappeared and small pores emerged at the same sites due to the previous dissolution of crystal particles on the macropore surfaces. These small, newly formed pores enabled the macropores to penetrate each other significantly, this contributed to new bone growth into the macropores [49].

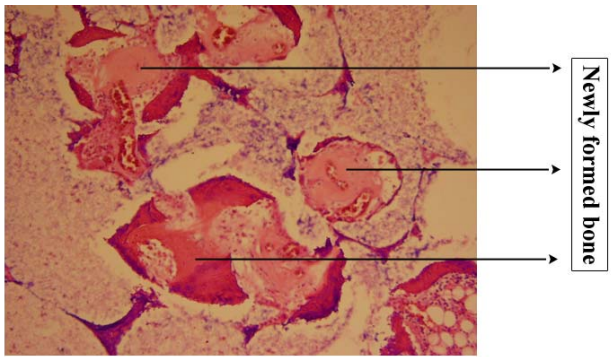

Fig. 9: Optical micrographs of C5 composite sample in an implant site 2 months post-operatively. (H.&E. magnification × 100)

4. CONCLUSIONS

In conclusion, the experiments provide data to support the use of the composite scaffolds in bone repair applications. Biomineralization studies showed that the deposition apatite phase on the surface of the scaffolds ascertaining the bioactive nature of the scaffolds. Also, the *in vitro* and *in vivo* results showed that the scaffolds were biocompatible, and no inflammation, tissue necroses, or tissue rejection was observed after implantation. The success of applying biomaterials composed of HAp and DCPD as scaffolds for generating a new bone tissue is related to the fact that this combination is biocompatible and forms a favourable three-dimensional matrix for human osteoblast cells to adhere and spread, associating the advantage of TCP osteoinduction to the superior bioactivity and osteoconduction of HAp.

References:

1. **W Suchanek, M. Yoshimura,** Processing and properties of hydroxyapatite-based biomaterials for use as hard tissue replacement implants, *J. Mater. Res.* **13** (1998) 94–117.
2. **F.J. Hou, S.M. Lang, S.J. Hoshaw,** D.A. Reimann, D.P. Fyhrie Human vertebral body apparent and hard tissue stiness, *J. Biomech.* **31**(1998) 1009-15.
3. **J.C. Runkle, J. Pugh,** The micro-mechanics of cancellous bone. II. Determination of the elastic modulus of individual trabeculae by a buckling analysis, Bull. Hosp. Jt Dis. 36 (1975) 2-10.
4. **P.R. Townsend, R.M. Rose,** E.L. Radin Buckling studies of single human trabeculae, *J. Biomech.* **8** (1975) 199-201.
5. **Kuhn JL, Goldstein SA, Choi K, London M,**

Feldkamp LA, Matthews LS. Comparison of the trabecular and cortical tissue moduli from human iliac crests. J Orthop Res 1989;7(6):876-84.

6. **Mente PL, Lewis JL.** Young's modulus of trabecular bone tissue. Transactions of the 33rd Annual Meeting on Orthopaedic Research Society, 1987. p. 49.

7. **J.Y. Rho, R.B. Ashman, C.H. Turner,** Young's modulus of trabecular and cortical bone material: ultrasonic and microtensile measurements, J. Biomech. 26 (1993) 111-9.

8. **O. Bermudez, M.G. Boltong, F.C.M. Driessens, J.A. Planell,** Compressive strengths and diametral tensile strength of some calcium- orthophosphate cements: a pilot study, *Mater. Sci. Mater. Med.* **4** (1993) 389-93.

9. **A.A. Al-Munajjed, N.A. Plunkett, J.P. Gleeson, T. Weber, C. Jungreuthmayer, T. Levingstone, J. Hammer, F.J. O'Brien,** Development of a biomimetic collagen–hydroxyapatite scaffold for bone tissue engineering using a SBF immersion technique, J. Biomed. *Mater. Res.,* **90**B (2009), pp. 584–591

10. **S. A. Poursamar, M. Azami, M. Mozafari,** Controllable synthesis and characterization of porous polyvinyl alcohol/hydroxyapatite nanocomposite scaffolds via an in situ colloidal technique, Colloids Surf. B: Biointerfaces (2011), doi:10.1016/j.colsurfb.2011.01.015

11. **R.M. Pilliar, M.J. Filiaggi, J.D. Wells, M.D. Grynpas, R.A. Kandel,** Porous calcium polyphosphate scaffolds for bone substitute applications—in vitro characterization. *Biomaterials* **22** (2001) 963–72.

12. **LeGeros RZ, LeGeros JP, Daculsi G, Kijkowska R.** Calcium phosphate biomaterials: preparation, properties and biodegradation. In: Wise DL, Trantolo DJ, Altobelli DE, Yaszemski MJ, Gresser JD, Schwartz ER, editors. Encyclopedic handbook of biomaterials and bioengineering, Part A: materials, vol. II. New York, USA: Marcel Dekker; 1995. p. 1429–63.

13. **Y. Zhang, M. Zhang,** Three-dimensional macroporous calcium phosphate bioceramics with nested chitosan sponges for load-bearing bone implants, *J Biomed Mater Res Part A,* **61** (2002), pp. 1–8.

14. **M. Mozafari, M. Rabiee, M. Azami, S. Maleknia**, Biomimetic formation of apatite on the surface of porous gelatin/bioactive glass nanocomposite scaffolds, Applied Surface Science 257 (2010) 1740-1749.

15. **Ducheyne P, Qiu Q.** Bioactive ceramics: the effect of surface reactivity on bone formation and bone cell function. Biomaterials 1999;20:2287–303.

16. **Suchanek W, Yoshimura M.** Processing and properties of hydroxyapatite-based biomaterials for use as hard tissue replacement implants. J Mater Res 1998;13(1):94–117.

17. **Wozney JM, Rosen V.** Bone morphogenetic protein and bone morphogenetic protein gene family in bone formation and repair. Clin Orthop Rel Res 1998;346:26–37.

18. **Asashina I, Watanabe M, Sakurai N, Mori M, Enomoto S.** Repair of bone defect in primate mandibule using a bone morphogenetic protein (BMP)–hydroxyapatite–collagen composite. J Med Dent Sci 1997;44:63–70.

19. **Burg KJL, Porter S, Kellam JF.** Biomaterial developments for bone tissue engineering. Biomaterials 2000;21:2347–59.

20. **Reddi AH.** Morphogenesis and tissue engineering of bone and cartilage: inductive signals, stem cells, and biomimetic materials. Tissue Eng 2000;6(4):351–9.

21. **Bruder SP,** FoxBS. Tissue engineering of bone. Clin Orthop Rel Res 1999;367S:S68–83.

22. **Boyan BD, Lohmann CH, Romero J.** Bone and cartilage tissue engineering. Clin Plast Surg 1999;26(4):629–45.

23. **S.Wongkhantee, V. Patanapiradej, C. Maneenut, D. Tantbirojn,** *J. Dent.* **34** (2006) 214.

24. **M.T. Fulmer, P.W. Brown,** J. Mater. Sci., *Mater. Med.* **9** (1998) 197.

25. **Raynaud, S., E. Champion, D. Bernache-Assollant, and P. Thomas** (2002) Calcium phosphate apatites with variable Ca/P atomic ratio I. Synthesis, characterisation and thermal stability of powders. *Biomaterials* **23**: 1065-1072.

26. **N. Kawai, S. Niwa, M. Sato, Y. Sato, Y. Suwa, I. Ichihara,** Bone formation by cells from femurs cultured among three-dimensionally arranged hydroxyapatite granules, *J Biomed Mater Res Part A,* **37** (1997), pp. 1–8.

27. **A. Hamlekhan, M. Mozafari, N. Nezafati, M. Azami, H. Hadipour,** "A proposed fabrication method of novel PCL-GEL-HAp nanocomposite scaffolds for bone tissue engineering applications", *Advanced Composites Letters,* **19** (2010), 123-130.

28. **N. Nezafati, F. Moztarzadeh, S. Hesaraki, M. Mozafari,** "Synergistically reinforcement of a self-setting calcium phosphate cement with bioactive glass fibers", Ceramics International (2010), doi:10.1016/j.ceramint.2010.11.002.

29. **L.L. Hench,** The story of Bioglass (R). *J. Mater. Sci. Mater. Med.* **17** (2006) 967-978.

30. **Hollinger, J. O., J. Brekke, E. Gruskin, and D.**

Lee (1996) Role of bone substitutes. Clin. Orthop. Relat. Res. 324: 55-65.

31. **Yamaguchi, K., T. Hirano, G. Yoshida, and K. Iwasaki** (1995) Degradation-resistant character of synthetic hydroxyapatite blocks filled in bone defects. *Biomaterials* 16: 983-985.

32. **Klein, C. P., H. van der Lubbe, A. A. Driessen, K. de Groot, and A. van den Hoof** (1983) Biodegradation behaviour of various calcium phosphate materials in subcutaneous tissue. pp. 356-368. In: P. Vincenzini (ed.). Ceramics in Surgery. Elsevier, Amsterdam, The Netherlands.

33. **Chu, T. M. G., D. G. Orton, S. J. Hollister, S. E. Feinberg, and J. W. Halloran** Mechanical and in vivo performance of hydroxyapatite implants with controlled architectures. *Biomaterials* **23**(2002) 1283-1293.

34. **Jarcho, M.** Calcium phosphate ceramics as hard tissue prosthetics. *Clin. Orthop. Relat. Res.* **157** (1981) 259-278.

35. **Vallet-Regi, M. and J. M. Gonzalez-Calbet** Calcium phosphates as substitution of bone tissues. *Prog. Solid State Chem.* **32** (2004) 1-31.

36. **L.L Hench,** bioceramics : from concept to clinic, *J.Am.Ceram. Soc.* **74**/7 1991 ,510-1487.

37. **Yubao, L., Klein, C. P. A. T., Xingdong, Z. and de Groot, K.,** Formation of a bone apatite-like layer on the surface of porous hydroxyapatite ceramics. *Biomaterials,* **15** 1994,835–841.

38. **Elliott, J. C.,** Structure and Chemistry of the Apatites and Other Calcium Orthophosphates.

39. Elsevier,Amsterdam, Netherlands, 1994. Lysaght MJ, Hazlehurst AL, Tissue engineering: The end of the beginning. Tissue Engineering, 10 (2004). 309-320

40. **Murugan R, Ramakrishna S.** Development of nanocomposites for bone grafting. Compos Sci Technol 2005; 65: 2385-406.

41. **Kim HW, Knowles JC, Kim HE.** Hydroxyapatite and gelatin composite foams processed via novel freezedrying and crosslinking for use as temporary hard tissue scaffolds. *J Biomed Mater Res Part A;* **72** 2005:136-45.

42. **R. Aoba and E.C. Moreno,** J. Dent. Res. 63 (1984), 874

43. **R.Z. Legeros and G. Daculsi,** in Handbook of bioactive ceramics edited T. Yamamuro, L.L. Hench and J. Wilson, CRC Press, Boca raton, 2/17 (1990)

44. **G. Daculsi, R.Z. Legeros and D. Mitre,** Calcified Tissue Int. 45, 95 (1989).

45. **I. Orly, M. Gregoire, M. Menanteau, M. Heughebaert and B. Kerebel,** Calcified Tissue Int. 45 (1989), 20

46. **R.Z. Legeros, R. Kijkowska, T. Abergas and J.P. Legeros,** J. Dent. Res. 65, 293 (1986).

47. **R.Z. Legeros and X. F. Chang,** J. Dent. Res. 68, 215 (1989).

48. **O. Malard, J.M. Bouler, J. Guicheux, D. Heymann, P. Pilet, C. Coquard, G. Daculsi, J. Biomed.** Mater. Res. 46, 103 (1999).

49. **Wang, J., W. Chen, Y. Li, S. Fan, J. Weng, and X. Zhang** (1998) Biological evaluation of biphasic calcium phosphate ceramic vertebral laminae. Biomaterials 19: 1387-1392.